SLAC-PUB-16898

$\mathcal{H}_2$-Optimal Transactive Control of Electric Power Regulation from Fast-Acting Demand Response in the Presence of High Renewables

David P. Chassin[a,b,*], Sahand Behboodi[b], Yang Shi[b], Ned Djilali[b,c]

[a] *SLAC National Accelerator Laboratory, Menlo Park, California (USA)*
[b] *Inst. for Integrated Energy Systems, and Dept. of Mechanical Engineering University of Victoria, Victoria, British Columbia (Canada)*
[c] *Renewable Energy Research Group, King Abdulaziz University, Jeddah (Saudi Arabia)*

Abstract

This paper presents an $\mathcal{H}_2$-optimal power regulation scheme for balancing authorities to provide regulation services using both generation and load resources in the presence of a significant amount of intermittent renewable generation. The optimal controller is designed to minimize the loss of total economic surplus due to deviations from the schedule because of generation contingencies. The results show that the optimal controller outperforms the conventional ACE control policy by 1) providing faster return to the schedule under varying demand response levels, 2) reducing the cost of using reserve units for regulation services, and 3) minimizing deviations from the global surplus-maximizing schedule.

Keywords: transactive control, power system control, frequency regulation, renewable intermittency, demand response

Highlights

- A transactive scheme that minimizes real-time operation deviations from schedule
- A model of fast acting demand response that provides frequency regulation service
- A robust control method that provides an economically-efficient use of load resources
- An $\mathcal{H}_2$-optimal control framework that outperforms the conventional ACE control policy

1. Introduction

Demand response is widely regarded as an important option for utilities to mitigate the intermittency of renewable generation resources [1]. System operator control of distributed loads is an emerging challenge in systems where demand response is expected to play a significant role in mitigating the adverse effects of renewable intermittency [2]. Transactive control has been proposed and demonstrated as an efficient approach to integrate demand response [3, 4]. Transactive control is a multi-scale and multi-temporal paradigm that can integrate wholesale energy, capacity, and regulation markets at the bulk system level with distribution operations, where demand response resource are aggregated and dispatched [5]. Under the transactive control paradigm, retail markets for energy, capacity, and regulation services are deployed to provide an analogous realization of wholesale markets at the distribution level. In spite of the conceptual similarity, the behavior of retail markets differs significantly from that of wholesale markets and remains an active area of research [6]. In particular, load behavior usually dominates the behavior of retail systems, which contrasts with wholesale systems where generation is dominant. In addition, there are a number of important processes in bulk power interconnection operations that have yet to be integrated fully into the transactive paradigm. Two very important such processes are system frequency regulation and control area import/export schedule tracking.

Frequency regulation and schedule tracking are jointly regulated using a tracking signal called "area control error" (ACE). The standard mechanism is based on a computation performed in time-domain independently in each control area by evaluating

$$[e(t) - e_s] + B[f(t) - f_s], \tag{1}$$

where e is the actual net exports from the control area, e_s is the scheduled net exports, B is the frequency bias, f is the interconnection frequency, and f_s is the nominal or scheduled frequency. Generators equipped with "automatic generation control" (AGC) respond proportionally to this ACE signal and adjust their output to compensate for both local and global under or over production. In parallel, load resources can also contribute to the power balancing, in particular considering their inherent capability for fast response to frequency deviations. Related to this we present a modification to control area balancing policy so that the grid operator can consider the load's

*Corresponding author
Email addresses: dchassin@slac.stanford.edu (David P. Chassin), behboodi@uvic.ca (Sahand Behboodi), yshi@uvic.ca (Yang Shi), ndjilali@uvic.ca (Ned Djilali)

This material is based upon work supported by the U.S. Department of Energy, Office of Science, under Contract No. DE-AC02-76SF00515.

response when dispatching generation assets and do so in a more economically efficient manner.

Numerous studies examining frequency regulation resource performance using diverse loads have been conducted in recent years. Lakshmanan et al. [8] studied the provision of secondary frequency control in electric power systems based on demand response activation on thermostatically controlled loads in domestic refrigerators in an islanded power system. Observations of household refrigerator response time, ramp rate, and consumer impact showed that they provide sufficient fast-acting demand response (FADR) resources for grid services, with a typical response time of 24 seconds and a p.u. ramp down rate of 0.63 per minute, which can satisfy the requirements for primary frequency control.

Zhong et al. [9] developed a coordinated control strategy for large-scale electric vehicles, battery storage and traditional frequency regulation resources for automatic generation control. Recognizing that response priorities and control strategies for these resources vary with different operating states they showed that a coordinated control approach not only fully utilizes each resource's advantages but also improves the frequency stability and facilitates the integration of renewable energy.

Falahati et al. [10] examined a model of storage using electric vehicles as moving batteries in deregulated power systems as one way to deal with the frequency regulation problem in a deregulated system with a growing share of intermittent generation resources. They enabled a vehicle-to-grid option for the control of the frequency using an optimized fuzzy controller to manage electric vehicle charging and discharging based on system frequency. The results illustrated satisfactory performance for frequency control of the grid system and verified the effectiveness of the approach at reducing the need for under-frequency load shedding to protect the system against large frequency excursions.

Teng et al. [11] proposed a framework to quantify and evaluate the impact of electric vehicles on island systems like Great Britain. This framework used a simplified power system model to analyze the effect of declining system inertia on primary frequency control and the ability of electric vehicle chargers and batteries to provide resources to mitigate that impact. Using this model they proposed an advanced stochastic system scheduling tool that explicitly models the loss of inertia and assesses the costs and emissions arising from primary frequency control as well as the benefits of having electric vehicles provide primary frequency response. In an analysis for Great Britain they showed that integrating electric vehicles in the primary frequency control system can significantly reduce anticipated cost and emissions growth.

Biel et al. [12] examined the frequency response of commercial HVAC systems by comparing different control strategies for providing frequency regulation demand response. Aside from significant impacts from intra-facility communications delay and control latencies, the authors did observe reductions in energy efficiency when the frequency regulation controls are more active, pointing to the necessity that the combined long-term energy cost and short-term regulation response revenue to be considered jointly. In a concurrent study, Khan et al. [13] followed up on studies by Hao [14] and Sanandaji [15] of the storage-like behavior of thermostatic loads by proposing a stochastic battery model. This model provides parameters of the battery model and considers changes to the hysteretic thermostatic control in response to frequency. This provides a relatively simple solution to load model aggregation. However the approach does not facilitate, or integrate easily with, transactive approaches, and does not properly account for the long-term endogenous energy integral error feedback that is intrinsic to thermostatic control in general.

A number of studies of optimal generation control designs have been previously reported. Bevrani and Bevrani [16] studied the general frequency control tuning problem for multiple objectives and proposed three methods for tuning PID controllers to improve the performance of closed-loop system, including a mixed $\mathcal{H}_2/\mathcal{H}_\infty$ optimal design method. This approach is easily transferable to a static output feedback control implementation, as is the case with ACE and any generalized extension where export schedule tracking is desired. The $\mathcal{H}_2$-optimal design method is particularly interesting when there are significant robustness issues to consider, although the authors did not present a solution to the synthesis of an optimal ACE controller.

The optimal ACE control design problem in the presence of significant demand response resources that autonomously respond to frequency deviations caused by intermittent generation has yet to be carefully examined. Autonomous frequency control using responsive loads was proposed by Schweppe et al. [18] and demonstrated in the US Department of Energy's Pacific Northwest Gridwise Demonstration testbed [19], which showed its potential to temporarily mitigate generation loss. Autonomous load control can provide much faster response to frequency deviations than generation resources or dispatched load control can. However the aggregate control gain and economic elasticity of responsive loads vary over time because these loads are typically thermostatic (e.g., waterheaters, heat-pump compressors) that have both time-of-day and weather sensitivities. Jay and Swarmy also recently proposed a reinforcement learning-based approach to automatic generation control that was found to minimize frequency deviations by incorporating thermostatic demand response control strategies [17]. Thus it seems necessary to investigate how the standard ACE control or the previously considered optimal ACE control designs would operate in the presence of autonomous demand response. We therefore propose an approach to regulating frequency and area exports that minimizes the global surplus impact of deviating from the schedule.

In Section 2 we introduce the interconnection operation control platform. We then present the methodology

for optimally controlling an area's response to system frequency deviations while tracking scheduled area exports. In Section 3 we propose the structure of the model and the design solution for an optimal area control policy. Finally in Section 4 we evaluate the performance of the optimal control policy when compared to the conventional control policy under varying demand response conditions.

2. Methodology

System operators that wish to use demand response resources to mitigate renewable intermittence must have the means to control responsive loads in much the same way they control responsive generating units. This can be done by updating the load control system gains every few minutes given the available demand response resources committed to frequency regulation. Given these load control gain settings, the loads' responses to frequency deviations can be autonomous without requiring the use of an analog to AGC for loads.

It is quite feasible with today's technology to dispatch load control gain settings to load aggregators who then disseminate specific setpoints to the loads they control without having to dispatch AGC signals to each load directly. However, doing so requires adjustments to the existing frequency and inter-area power exchange control system. This section details how this is accomplished given the structure of modern power system control.

2.1. Frequency control mechanism

Primary control of bulk electric power systems is driven in part by deviations in frequency at the system level and modeled by the system transfer function $\frac{1}{Ms+D}$, where M represents the system's inertial response and D represent the system's damping response. Each control area implements a combination of speed-droop control on conventional generating units, under-frequency load shedding, and grid-friendly loads to provide primary control. Renewable generating units provide no frequency regulation capability because they cannot control their prime movers (wind and solar). Secondary control of frequency and area exports is provided by units equipped with master controllers and is based on the area control signal a using the conventional ACE formula

$$a(t) = \Delta_e(t) + B\Delta_f(t), \tag{2}$$

where a is the raw ACE signal, $\Delta_e(t) = e(t) - e_s$ is the deviation of the net power exports from the scheduled net exports over tie lines and $\Delta_f(t) = f(t) - f_s$ is the interconnection's frequency deviation from scheduled frequency. In most realizations the ACE signal is updated by the SCADA system about every 4 seconds and further passed through a smoothing filter so that it changes with a time-constant well in excess of the generating units' fastest response, e.g., 30-90 seconds, with the purpose of reducing wear and tear on generating unit governor motors and turbine valves [7].

If an area's net exports deviates from its schedule (because of either an internal or external disturbance), the area adjusts its generation and potentially load such that it eventually will zero out $a(t)$, while also providing adjustments necessary to support system-wide corrections to frequency deviation. In most realizations the raw ACE signal is updated by the SCADA system about every 4 seconds and further passed through a smoothing filter to avoid over-actuation of generating units that could cause reducing wear and tear on generating unit governor motors and turbine valves [7]. In addition, this control action is subject to control performance standards (i.e., CPS 1 and 2 [20]), although these are not considered in this study.

The fast response of frequency-sensitive loads (grid-friendly smart appliances) to the frequency deviation enables the grid operator to redispatch generation units in a more economically-efficient manner, although demand response may saturate relatively quickly. Fig. 1 illustrates the system's frequency regulation diagram with variable renewable generation and frequency sensitive demand response.

2.2. Transactive control platform

The question of what constitutes optimality is complicated by the lack of consensus in the definition of "transactive" control [21]. For this study we use the definition of transactive preferred by Fuller et al. for its generality and simplicity [22]:

> *Utilizing a central control and distributed agent methodology [...] to act on behalf of consumers, sending information and automatically adjusting settings in response to a centralized signal.*

This definition does not specify any particular physical or temporal control architecture. We use the hierarchy defined in [23] and illustrated in Fig. 2, which fits well with Fuller's definition and provides a relatively simple data flow between physical and temporal scales. Using this approach the total generation and load is scheduled hourly such that for each control area a uniform price is obtained at which supply is equal to load plus net exports. Fig. 3 illustrates an interconnection including N wholesale markets each belongs to a control area that exchange electricity through system tielines to increase the economic surplus. This schedule is used to set each area's price ψ_s and net exports e_s which are in turn used by 5-minute dispatch markets [3] to reallocate resources in response to deviations from the hourly schedule. Depending on the events that have occurred during the preceding 5-minute time period, the state of operation of generators and loads at the end of the period is not necessarily the same as at the beginning of the period. For example, the water temperature of a hot water tank whose heater was switched off at the last time period has lowered, and we expect this load might submit a higher bid to the market to avoid staying in the off mode and satisfy a higher level of demand urgency. Accordingly,

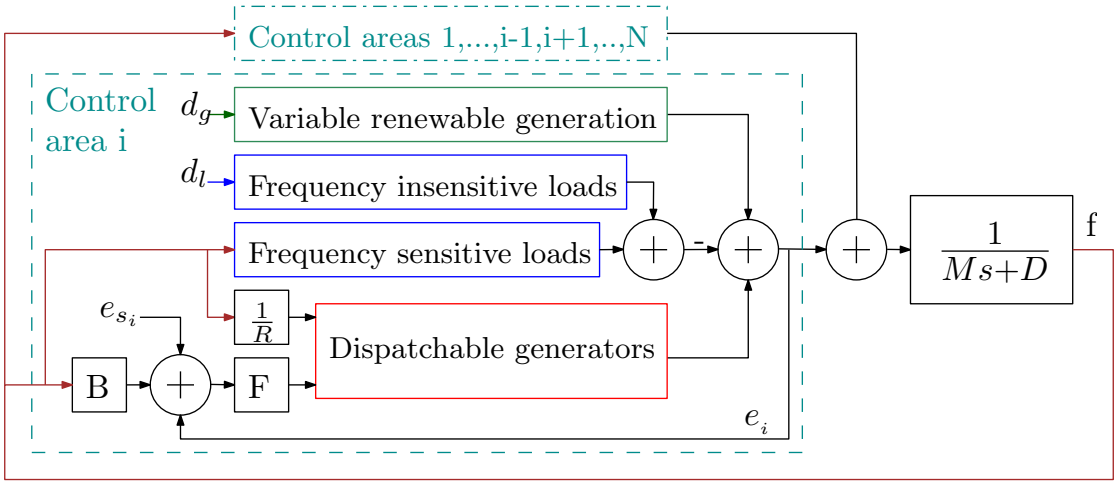

Figure 1: System frequency control diagram.

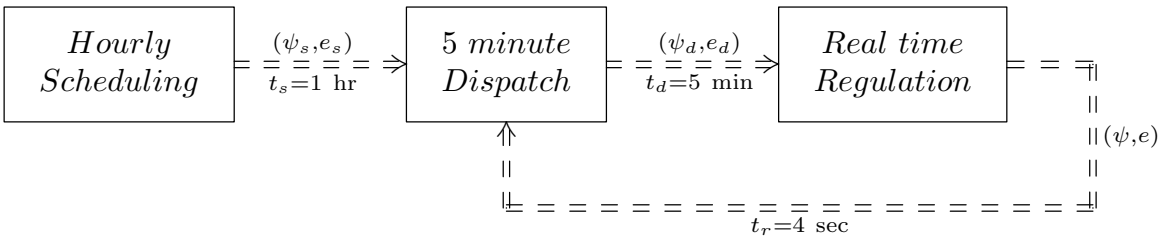

Figure 2: Transactive inter-temporal data flow diagram.

generation and load resources may participate in the market with new bid prices, and as a result the clearing price ψ_d would change. However, the area export e_a should remain as close as possible to the hourly schedule.

The transactive control dispatch system is used to solve two concurrent problems.

(i) **Schedule tracking**: The hourly schedule is set by the unit commitment process [24] at the interconnection level. From this process we obtain the schedule price ψ_s that is determined from the hour-ahead supply and demand bids, and corresponds to the control area's net export schedule e_s, which will be the control reference for dispatching units over the coming hour. The implementation of solutions to the scheduling surplus maximization problem in the interconnection scale is addressed in [25]. Any deviation from the scheduled export should be avoided because it may pose a reliability issue elsewhere in the interconnection and result in economic losses throughout the interconnection.

(ii) **Resource dispatch**: Every five minutes generation and load resources are dispatched and the regulation control is reset to establish the basis for the control of system frequency and area exports over the next 5-minute interval. Units with non-zero participation factors bid into the dispatch market to allow the schedule to be adjusted so that recent resource state changes can be considered. Contribution and participation factors are computed and used (a) to reset the power output for generation units, (b) to reset the state of demand response, and (c) set the frequency regulation gain for both generation and demand response.

Because we wish to consider the behavior of the system when demand response is active, we are motivated to find an optimal control policy that maintains the maximum total economic surplus established by the schedule. Based on the transactive system design demonstrated by Hammerstrom et al. [19], Kiani and Annaswamy [26] proposed a hierarchical transactive control model for renewable integration that incorporates primary, secondary and tertiary frequency control that is consistent with the architecture in Fig. 2. This model was successful in not only describing the primary regulation response of steam turbines to a loss of wind using a transactive model, but also the disequilibrium process of the secondary and tertiary responses. Because transactive control incorporates economic signals, Kiani's model can be used to evaluate the impacts of transactive controls on total economic surplus both with and without their proposed tertiary control. Evaluating the surplus impacts provides an useful alternative to the typical optimization objective of minimizing frequency deviations, generator response, or regulation cost, especially in the context of transactive controls where the joint energy, power, and ramp responses have different time-varying cost functions and are considered over different time-horizons.

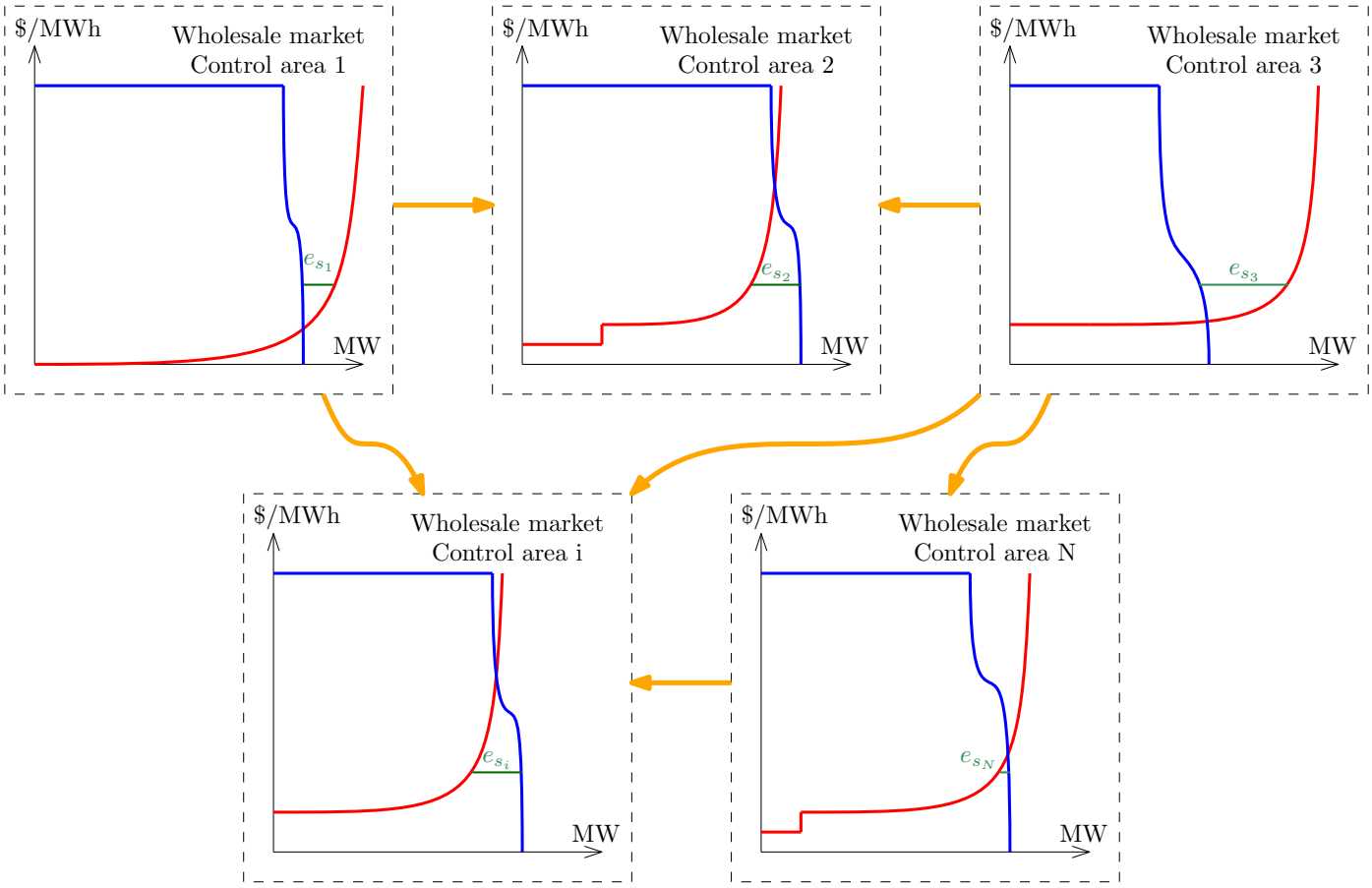

Figure 3: Inter-area transfer flows within an interconnected system consisting of N control areas.

With both the scheduling and dispatch strategies available we have all the necessary elements required to consider a regulation response strategy that minimizes schedule deviation and tracks the surplus maximizing schedule adjusted by the last 5-minute redispatch operation. The goal is to minimize the initial over-production of power, which reduces later under-production and allows the system to track its schedule more smoothly and cost-effectively. We therefore focus on one specific aspect of the larger transactive control design problem, namely the integration of the 5-minute dispatch control with the automatic control mechanism that regulates system frequency in the presence of demand resources that are frequency sensitive [27].

2.3. Demand response integration in the 5-minute market

Fig. 4 illustrates the impact of a supply disturbance on the 5-minute market settlement process. The blue and the red dashed curves represent the demand and the supply curves, respectively, in the next market cycle. In this event, a portion of renewable generation (in the flat segment of supply curve) is lost; therefore supply curve is shifted to left by the magnitude of the disturbance d_p[1]. Load participation in frequency response prior to the redispatch operation

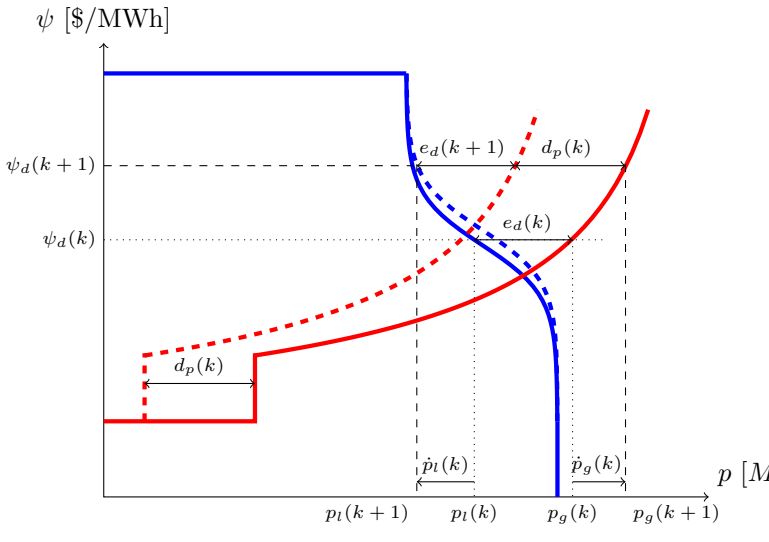

Figure 4: Five-minute resource dispatch with supply (red) and demand (blue) response to a loss of generation (d_p).

causes the shape of demand curve to change slightly and

[1]Other kinds of disturbances include non-renewable generation loss or changes in load, and these will have similar impact with only particular details differing. The choice of renewable generation loss is preferred in this study because (i) it is a common concern for which demand response is often cited as a potential solution, and (ii) it

represent the remaining available demand response to the 5-minute redispatch market. Moving from the market k to the market $k+1$, the clearing price increases from $\psi_d(k)$ to $\psi_d(k+1)$ so that the dispatched load changes by $\dot{p}_l(k) = p_l(k+1) - p_l(k) = (1-\alpha)d_p(k)$ and the dispatched generation changes by $\dot{p}_g(k) = p_g(k+1) - p_g(k) = -\alpha d_p(k)$ where $0 \leq \alpha \leq 1$ to satisfy the physical constraint that $\dot{p}_g(k) - \dot{p}_l(k) = -d_p(k)$ or $e_d(k+1) = e_d(k) = e_s$.

To respond efficiently to a frequency deviation, generation units must change their output by $\dot{p}_g(k)$ as their contribution to restoring the area's export power to the committed hourly-scheduled level, as shown in Fig. 5. Concurrently load must change demand by $\dot{p}_l(k)$ as their contribution to efficiently restoring system frequency. The

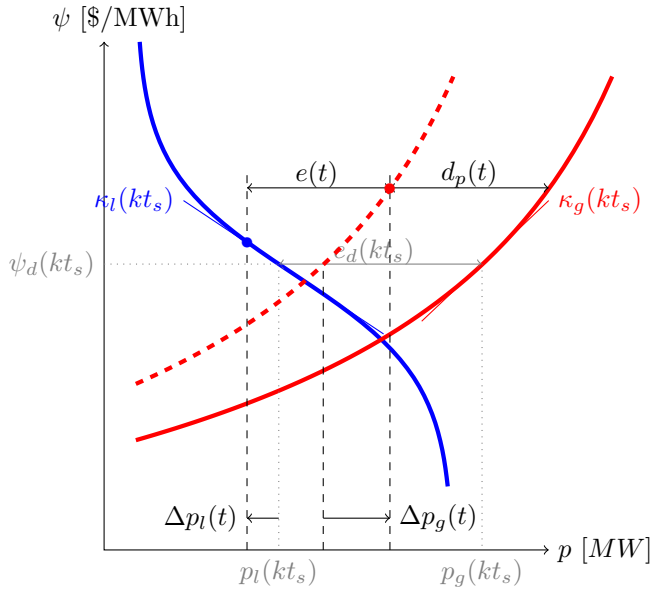

Figure 5: Real-time response of generation and load to a disturbance.

export power error at the time t is $\Delta e(t) = e(t) - e_d(kt_d) = d_p(kt_d) + p_g(t) - p_l(t)$. The economically optimal response is that for which the marginal cost of the generation response is equal to the marginal cost of the demand response. We compute the regulation response price, $\psi(t)$ to quantify the marginal cost of deviations from the hourly schedule in real time:

$$\psi(t) = \psi_d(kt_d) + \frac{\kappa_g(kt_d)\ \kappa_l(kt_d)}{\kappa_l(kt_d) - \kappa_g(kt_d)} \Delta e(t).$$

where $\kappa_g(kt_d)$ and $\kappa_l(kt_d)$ are the slopes of the generation supply and load demand curves at the time of dispatch kt_d, respectively, for the redispatch exports $e_d(kt_d)$ for the next 5 minutes, and $e(t)$ is the actual exports at the time t. In the 5-minute dispatch market k, $e_d(k)$, $\kappa_g(k) > 0$ and $\kappa_l(k) < 0$ are updated every 5-minutes.

provides a clearer illustration of the various effects on transactive system behavior.

At the system level a deviation in net power will be associated with a deviation in frequency as well, regardless of whether the power deviation is endogenous to the local control area. For this reason we incorporate two additional cost components, one for the frequency deviation itself and the other for the control response arising from the ACE signal. The net cost taken over the entire system is zero in the sense that the payments made to areas mitigating a deviation are equal to payments by the areas contributing to it.

The total balance of payments is

$$\int_0^{300} \psi_d[\Delta_e(t) + B\Delta_f(t)] - \psi(t)[a(t) - d_p(t)]dt, \qquad (3)$$

where $\psi(t)$ is the cost of the over/under-response to the ACE signal $a(t)$ as a result of the disturbance $d_p(t)$. The value of $\psi(t)$ will depend on the mix of generation (e.g., hydro, coal, nuclear, combine cycle gas turbine) that responds to the ACE signal. Any non-zero payments by any party represents a deviation from the surplus-maximizing condition represented by the schedule and therefore represents a loss of surplus. Our objective then is to minimize these payments by expressing them as a weighted squared sum of the three cost components, Bf, p, and $\psi(t)(a - d_p)/\psi_d$. This 2-norm minimization in the wake of a generation contingency of magnitude d_p is expressed by the objective

$$\min_{a(t)} \int_0^{300} \omega_1[\Delta_f(t)]^2 + \omega_2\Delta_e^2(t) + \omega_3\left(a(t) - d_p(t)\right)^2 dt. \quad (4)$$

where $\omega_1 = B$, $\omega_2 = 1$ and $\omega_3 = \frac{\psi(t)}{\psi_d}$.

When this objective is satisfied, we can be assured that we have also maximized the total surplus given the prevailing conditions: by minimizing the individual payments or receipts on both sides of the balance of payments we have minimized the deviation from the surplus-maximizing schedule and therefore minimized the surplus loss due to regulation.

2.4. $\mathcal{H}_2$-optimal control policy

We have the conditions necessary to synthesize the $\mathcal{H}_2$-optimal control policy for a control area that minimizes the costs associated with operating the system as it returns to the scheduled set-point, including frequency regulation in the presence of FADR resources. We now require the individual component models within the control area used to synthesize the optimal control policy.

We now introduce the state-space solution of the $\mathcal{H}_2$-optimal control problem [28]. We consider the standard control system in Figure 6 and we partition of the plant G according to

$$\begin{bmatrix} z \\ y \end{bmatrix} = \begin{bmatrix} G_{11} & G_{12} \\ G_{21} & G_{22} \end{bmatrix} \begin{bmatrix} v \\ u \end{bmatrix}.$$

The closed-loop system has the transfer function

$$z = F(G, K)v$$

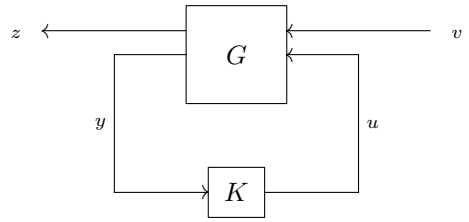

Figure 6: Standard system for $\mathcal{H}_2$-optimal control synthesis

where $F(G,K) = G_{11} + G_{12}(I - KG_{22})^{-1} + KG_{21}$. The $\mathcal{H}_2$-optimal control problem consists of finding the causal controller K that stabilizes the plant G while minimizing the cost function

$$J_2(K) = ||F(G,K)||_2^2$$

where $||F(G,K)||_2$ is the $\mathcal{H}_2$ norm of the transfer function from v to z.

To obtain this transfer function we begin with non-dispatchable generation, primarily wind and solar resources. These resources do not contribute to either droop or ACE-control responses and have null responses to both frequency and ACE signal. The fraction of non-dispatchable generation in the study area is denoted F_w and for the design case we will use 75% renewable resource penetration to exemplify an extreme situation.

The thermal generating unit response to the filtered area generation control signal a_s is given by the simplified transfer function [7]

$$G_r(s) = \frac{\hat{g}_r(s)}{\hat{a}_s(s)} = \frac{1}{(1+sT_g)(1+sT_{ch})}, \tag{5a}$$

where $\hat{g}_r$ is the thermal unit's output, T_g is the governor time constant and T_{ch} is the time constant of the steam chest. Typical values for steam turbine units are [7]

$$T_{ch} = 0.3 \text{ sec} \qquad \text{and} \qquad T_g = 0.2 \text{ sec},$$

which gives the ACE-controlled generation response transfer function

$$G_r(s) = \frac{16.7}{(s+5.00)(s+3.33)}. \tag{5b}$$

The fraction of units that respond to the area generation control signal is denoted F_r which is set to 25% for the design case. All dispatchable units that do not respond to area control are provided with droop response such that [7]

$$G_d(s) = \frac{\hat{g}_d(s)}{\hat{f}(s)} = \frac{1}{R}G_r(s), \tag{5c}$$

where $\hat{g}_d$ is the droop-controlled unit's output and $R = -0.05$ is the conventional frequency droop response of generating units. Given that we have selected a design case with the extreme of 75% renewable generation, we expect the number of droop units to be zero and this component is omitted from the design case model.

The filtered area generation control signal a_s is computed by sending the raw ACE signal through a low pass filter F to avoid excessive actuation of the regulating units. For the purposes of this study the values

$$B = 21 \qquad \text{and} \qquad F(s) = \frac{1}{1+sT_f}, \tag{5d}$$

are used with $T_f = 0.02$ seconds.

Based on data obtained from field tests [19], the conventional grid-friendly control response exhibits two important behaviors. The first behavior is the primary underfrequency event response, which acts like a strong derivative response reaching maximum within a few seconds followed by a very slow recovery using integral error feedback over a period of a minute or more. These are approximated satisfactorily using the demand response transfer function

$$L(s) = \frac{\hat{l}(s)}{\hat{f}(s)} = \frac{F_d K_d s + K_p}{T_l s^2 + s + K_l}, \tag{5e}$$

where $\hat{l}$ is the load response, F_d is the fraction of total load that is responsive, and for the design condition $K_d = 1/F_d$ is the fraction of responsive load that is armed by the 5-minute redispatch[2], and K_p is the quasi-steady state rebound response. The derivative response time constant $T_l = 0.17$ seconds and the recovery time constant $K_l = 0.01$ per second are based on the responses observed in the grid-friendly controllers studied in the US Department of Energy's Olympic Peninsula GridWise testbed [19]. This gives us

$$L(s) = \frac{59s}{(s+5.8)(s+0.1)}, \tag{5f}$$

as the general fast-acting demand response transfer function. The response of the loads is initially very fast and very strong, but it decays within a few minutes, and it is therefore minimally described as a second-order response with derivative control. The rebound response K_p is excluded in this model because it is expected to be addressed by the redispatch operation after a maximum of 5 minutes. The load response is therefore not net-energy neutral over the 5-minute period. This allows us to suppress the non-minimum phase behavior that can emerge from thermostatic loads when their curtailment signal is released and they settle into a higher load condition for a prolonged demand response rebound period. For the controller design condition we use 5% controllable load resources, but the total demand response availability is varied from 0% to 50% for the control robustness analysis below.

The interconnected system's overall response to net power deviations is given by the damped inertial response transfer function

$$H(s) = \frac{\hat{f}(s)}{\hat{p}(s)} = \frac{1}{Ms + D}, \tag{5g}$$

[2]Note $K_D F_D$ is unity at 5% DR but when F_D is changed K_D is not changed.

where $\hat{p}$ is the response of all system generator output power , $D = 1$ is a typical value for the load damping constant, and $M = 6$ is a typical value for the system with somewhat low inertia [7].

Fig. 7 illustrates the system. Each control area is modeled with: (1) loads L controlled by frequency through the controller K_L/R; (2) frequency droop generators G_d controlled by the droop gain K_G/R, and (3) ACE-controlled generators using the controller K which we will design. The ACE input to the controller K considers the frequency droop $-1/R$, system damping D, and the export error $E_A - E_S$, while the frequency is obtained the system inertial response $1/(Ms + D)$. The frequency input to ACE is defined as the bias $B = D - 1/R$.

The interconnected system's open-loop frequency, generation and load responses to a nearly step disturbance are shown in Fig. 8. For the design condition we have set the demand response control gain to match the generation control gain as expected from the 5-minute market dispatch of the regulation contribution factors.

3. Implementation

We can now consider the $\mathcal{H}_2$-optimal control design problem [29] for the system shown in Fig. 7 and arranged in the standard form shown in Fig. 9. The controller K provides coordinated dispatch of regulation response for generation resources G_r. The controller measures the system frequency f and the control area's net export schedule power deviation p. The current ACE control policy from Eq. (2) is the baseline control policy for this study. The frequency bias B is computed based on the generation and load characteristics of the control area [7].

A 5% generation local loss input disturbance is modeled as very nearly a step-loss of generation in the local control area. The input filter for the power disturbance is thus specified as

$$\hat{d}_p(s) = \frac{20d}{s^2 + 20s + 0.01}, \tag{6a}$$

where d is the magnitude of the disturbance, which for this study is set at 5% of the total system load. This magnitude disturbance corresponds results in a deviation of $\Delta f = \lim_{x\to\infty} \frac{-d}{D}(1 - e^{-\frac{D}{M}t}) \times f_0 = 3.0$ Hz, which is very significant for a 60 Hz system. This may seem like a large disturbance for a North American system. But it is not atypical for systems in other parts of the world or for microgrids. Demonstrating the effectiveness of transactive control in such systems in useful and therefore a large disturbance is considered. The remaining disturbances are taken as frequency and power measurement noise of magnitude of 1%.

The optimization seeks to minimize regulation deviations from the economically optimal schedule given by the most recent 5-minute dispatch of frequency responsive generation and load resources. Because the maximum surplus is achieved when the dispatch schedule is followed, any deviation from the schedule will reduce the total surplus. We therefore construct the $\mathcal{H}_2$ control output vector components

$$z(t) = \begin{bmatrix} c_a(t) \\ c_p(t) \\ c_f(t) \end{bmatrix} = \begin{bmatrix} \frac{\psi(t)}{\psi_d}[a(t) - d_p(t)] \\ Cp(t) \\ Bf(t) \end{bmatrix}, \tag{6b}$$

the 2-norm of which we will seek to minimize. The transfer function for the energy cost impact is given as nearly an integrator in the sense that it costs slightly more to provide an early generation response than a late one. The energy cost transfer function is approximated as

$$\hat{c} = \frac{1}{s^2 + 20s + 0.01}. \tag{6c}$$

The value $\psi(t)$ is given in units of \$/MWh and B is given in units of MW/Hz.

The measurement outputs for power and frequency $y(t) = \left[\begin{smallmatrix} p(t) \\ f(t) \end{smallmatrix}\right]$ are taken directly from the system and the generation+load+disturbance outputs, respectively to which the input disturbance noises are added.

The control input for the raw area control signal is $u(t) = \left[a(t)\right]$ and will either be the ACE control signal

$$\hat{a} = \tfrac{1}{s}\hat{p} + B\hat{f} \tag{6d}$$

for the baseline model, or the $\mathcal{H}_2$-optimal controller output as described below for the study model.

3.1. State-space realization

Using the packed matrix notation $G = \left[\begin{smallmatrix} \mathbf{A} & \mathbf{B} \\ \hline \mathbf{C} & \mathbf{D} \end{smallmatrix}\right] = \mathbf{D} + \mathbf{C}(s\mathbf{I} - \mathbf{A})^{-1}\mathbf{B}$ we obtain the state-space realization for the study model of the control area given by Eq. (7a).

$$G = \left[\begin{array}{cccccccccc|ccc}
-0.1667 & 0 & 1.0417 & -1.4706 & 0 & 0 & -1 & 0 & 0 & 0 & 0.005 & 0 & 0 \\
0 & -8.3333 & -4.1667 & 0 & 0 & 0 & 0 & 0 & 0 & 0.1333 & 0 & 0 & 0 \\
0 & 4 & 0 & 0 & 0 & 0 & 0 & 0 & 0 & 0 & 0 & 0 & 0 \\
0.6667 & 0 & 0 & -5.8824 & -0.2353 & 0 & 0 & 0 & 0 & 0 & 0 & 0 & 0 \\
0 & 0 & 0 & 0.25 & 0 & 0 & 0 & 0 & 0 & 0 & 0 & 0 & 0 \\
0 & 0 & 0 & 0 & 0 & -20 & -0.08 & 0 & 0 & 0 & 4 & 0 & 0 \\
0 & 0 & 0 & 0 & 0 & 0.125 & 0 & 0 & 0 & 0 & 0 & 0 & 0 \\
0 & 0 & 8.3333 & -11.7647 & 0 & 0 & -8 & -20 & -0.08 & 0 & 0 & 0 & 0 \\
0 & 0 & 0 & 0 & 0 & 0 & 0 & 0.125 & 0 & 0 & 0 & 0 & 0 \\
0 & 0 & 0 & 0 & 0 & 0 & 0 & 0 & 0 & -0.0167 & 0 & 0 & 0.0625 \\
\hline
0 & 0 & 0 & 0 & 0 & 0 & 0 & 0 & 0 & 0 & 0 & 0 & 1 \\
0 & 0 & 0 & 0 & 0 & 0 & 0 & 0 & 2 & 0 & 0 & 0 & 0 \\
7 & 0 & 0 & 0 & 0 & 0 & 0 & 0 & 0 & 0 & 0 & 0 & 0 \\
0 & 0 & 2.0833 & -2.9412 & 0 & 0 & -2 & 0 & 0 & 0 & 0.01 & 0 & 0 \\
0.3333 & 0 & 0 & 0 & 0 & 0 & 0 & 0 & 0 & 0 & 0 & 0.01 & 0
\end{array}\right], \tag{7a}$$

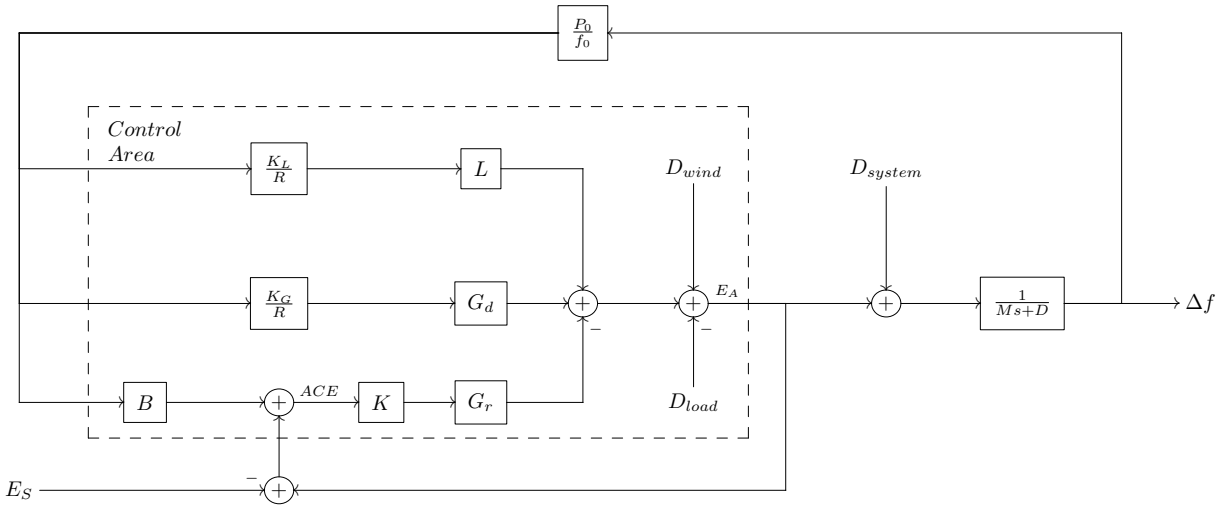

Figure 7: System frequency and control area export regulation control diagram.

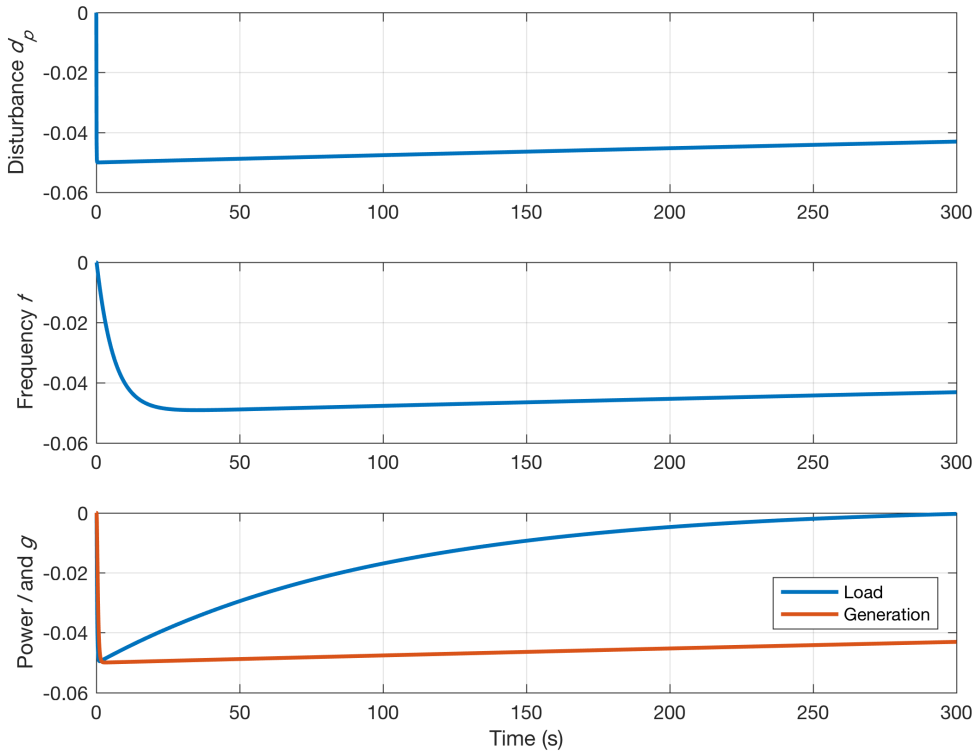

Figure 8: Model component frequency (f p.u. nominal frequency), load (l p.u. area load) and generation (g p.u. system load) responses to a local disturbance (d_p p.u. system load).

which yields the synthesized $\mathcal{H}_2$-optimal regulation policy for the control area

$$K = \left[\begin{array}{cccccccccc|cc} -0.1667 & 0 & 0 & 0 & 0 & 0 & 0 & 0 & 0 & 0 & 0.5 & 0 \\ 0 & -8.3333 & -4.1667 & 0 & 0 & 0 & 0 & 0 & 0 & 0.1333 & 0 & 0 \\ 0 & 4 & 0 & -0 & 0 & 0 & -0 & 0 & 0 & 0 & -0 & 0 \\ 0.6667 & 0 & -0 & -5.8824 & -0.2353 & 0 & 0 & 0 & 0 & 0 & 0 & 0 \\ 0 & 0 & -0 & 0.25 & 0 & 0 & 0 & 0 & 0 & 0 & 0 & 0 \\ 0 & 0 & -547.427 & 772.839 & 0 & -20 & 525.45 & 0 & 0 & 0 & 262.765 & 0 \\ 0 & 0 & 8.6287 & -12.1817 & 0 & 0.125 & -8.2836 & 0 & 0 & 0 & -4.1418 & 0 \\ 0 & 0 & 5.4743 & -7.7284 & 0 & 0 & -5.2553 & -20 & -0.08 & 0 & 1.3723 & 0 \\ 0 & 0 & -0.0863 & 0.1218 & 0 & 0 & 0.0828 & 0.125 & 0 & 0 & 0.0414 & 0 \\ -0.024 & -0.0082 & -0.0166 & 0.0047 & -0.0667 & 0.0091 & 1.4543 & -0.0006 & -0.1 & -0.0496 & 0 & 0 \\ \hline -0.3843 & -0.1308 & -0.2652 & 0.0759 & -1.0671 & 0.1453 & 23.2695 & -0.01 & -1.6002 & -0.5265 & 0 & 0 \end{array}\right], \quad (7b)$$

and the corresponding transfer function from power p to area control a

$$\frac{-58.472(s+20)^2(s+5.6947)(s+5)(s+3.3333)(s+0.3625)(s+0.016667)(s+0.0086675)(s+0.0023866)}{(s+24.142)(s+19.999)(s+5.8723)(s+5.2747)(s^2+7.2484s+13.55)(s+0.16667)(s+0.010017)(s+0.0015464)}. \quad (7c)$$

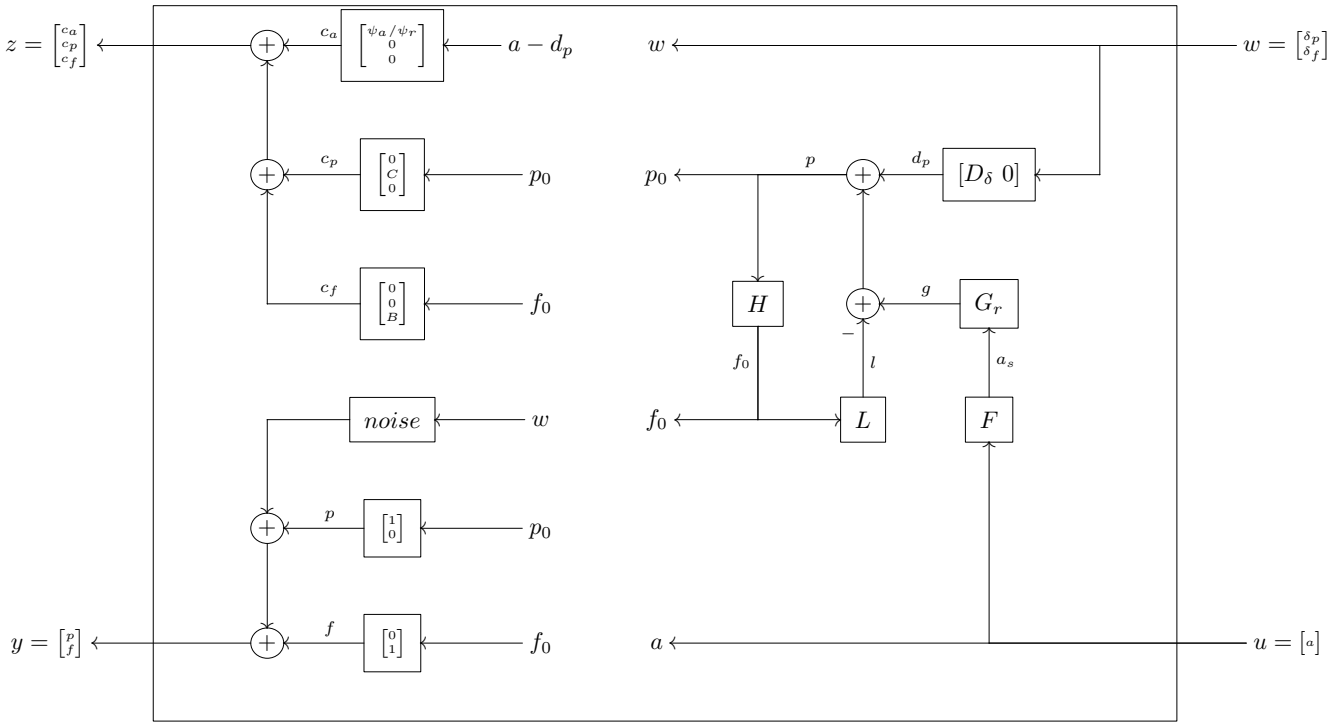

Figure 9: Control area model in standard form.

The smallest eigenvalue of the closed-loop system GK is -0.0005 and there are no complex conjugate poles. Unlike the ACE control policy, the $\mathcal{H}_2$-optimal area control policy does not rely on a frequency input and only requires measurement of net exports from the control area. By way of comparison, the conventional ACE control state-space model is given by

$$K_A = \left[\begin{array}{c|cc} 0 & 1 & 0 \\ \hline 1 & 0 & B \end{array}\right], \tag{8}$$

where $B = D - 1/R = 21$, which is used for the baseline model. The smallest eigenvalue of the closed-loop system GK_A is -0.0005 and it has a single pair of complex conjugate poles at $-0.0367 \pm 0.0343j$.

3.2. Model Validation

The model of ACE control is verified for varying amounts of demand response under the design conditions, as illustrated in Fig. 10. The ACE response is adequate for the conditions given insofar as it restores both frequency and power within about 120 seconds of the initial event. The $\mathcal{H}_2$-optimal control response fully restores both frequency and power to zero but with significantly less overshoot. Although it does not occur in this particular study, we anticipate that any residual transient error that persists at the end of a 5-minute dispatch interval will be corrected after the next dispatch or scheduling operation.

The area control signal (a) for $\mathcal{H}_2$-optimal control is initially faster in its response to the initial event but of lesser magnitude. The power and frequency responses, (p

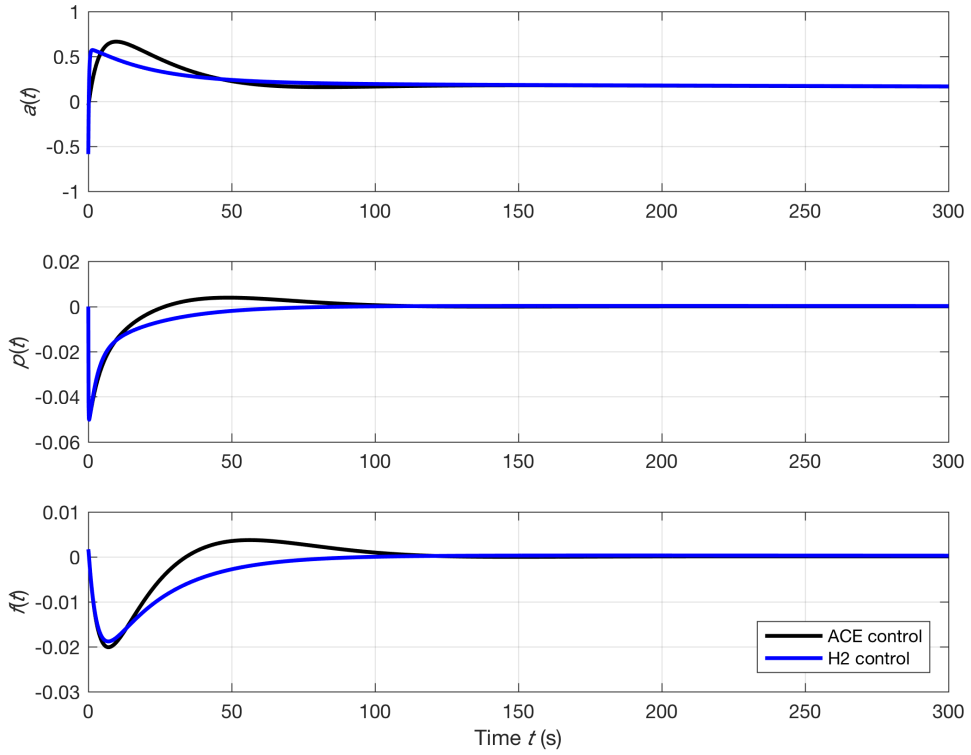

Figure 10: ACE control (black) and $\mathcal{H}_2$-optimal (blue) control performance for design conditions (5% FADR), showing the raw ACE signal (a p.u. area load), area generation output (p p.u. system load), and system frequency (f p.u. nominal frequency) response to a loss of generation within the control area.

and f, respectively) are very similar for the first 10 seconds following the event. However afterwards the power and frequency response to $\mathcal{H}_2$-optimal control signal is reduced to minimize costly overshoot.

The steady-state power and frequency deviation for both control policies is zero and both achieve steady-state in approximately the same time. As a result, the area control signal reaches the same steady-state value for both control policies.

4. Control Performance

We recognize that demand response resource availability can vary widely from one area to another, from hour to hour, and from season to season. Thus we evaluate the performance of the $\mathcal{H}_2$-optimal control policy relative to the conventional ACE control policy by comparing the response of each to widely varying demand response resource availability. The area generation control signal, net power exports and system frequency are compared for a 100 MW load base control area with a nominal energy price of \$100/MWh. In addition, the cost of regulation and energy used for regulation are compared.

The disturbance response of generation (p per unit area load) and load (l per unit area load) are shown in Fig. 11 for the conventional ACE signal (left) and $\mathcal{H}_2$-optimal control (right). In addition, the generation control cost c_g is shown in units of \$/h per unit area load. We observe decreasing stability of the ACE control policy under higher penetration of fast-acting demand response. This phenomenon is consistent with previously observed results for load controller delays that exceed 1/4 second [30]. In contrast the $\mathcal{H}_2$-optimal control policy exhibits less oscillation and shorter settling-time performance indicating that it is much less susceptible to overall performance degradation under high demand response scenarios. In every other important respect, and particularly with respect to the steady-state, the $\mathcal{H}_2$-optimal control policy is comparable to the ACE control policy.

The comparative costs contribution to the objective function are presented in Fig. 12. The ACE control policy exhibits significantly more deviations from the schedule, particularly under high demand response conditions and is unable to establish a steady regulation regime under high demand response. In all conditions ranging from no demand response to 50% demand response, the $\mathcal{H}_2$-optimal control policy establishing a steady regulation regime that zeros out the deviation of operation from the surplus maximized schedule within about 150-200 seconds.

The cost savings and energy impacts from utilizing $\mathcal{H}_2$-optimal control are shown in Table 1. It is noteworthy that in all cases generation and energy costs are reduced,

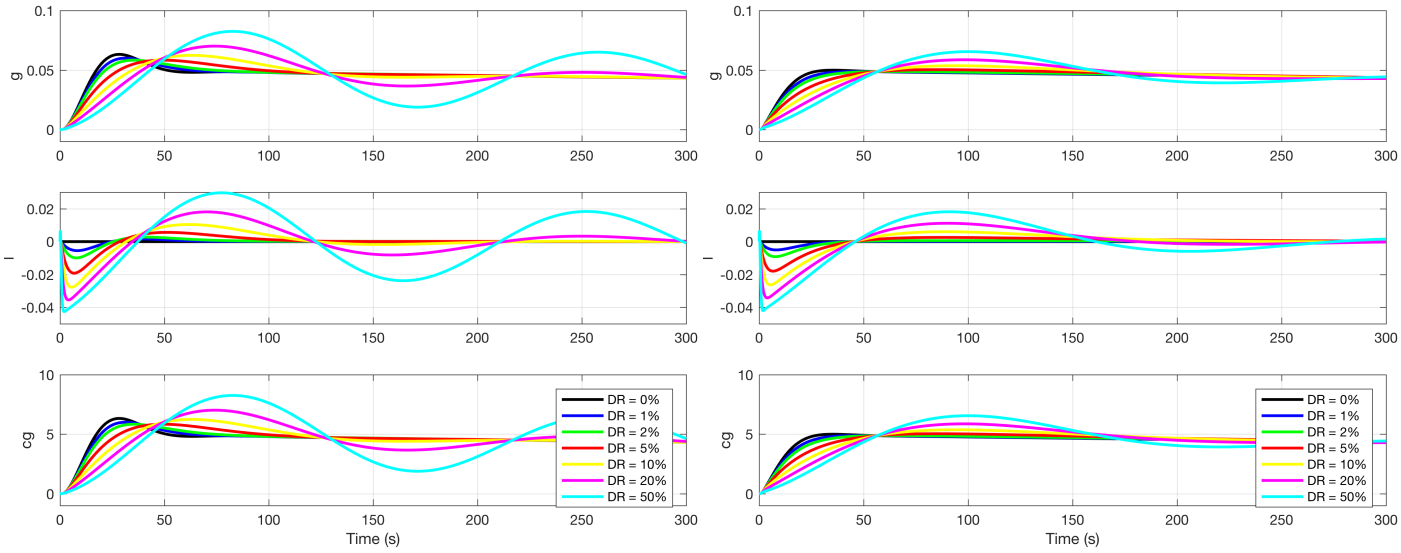

Figure 11: ACE control (left) and $\mathcal{H}_2$-optimal control (right) model validation for varying demand response level with generation response (g p.u. area load), demand response (l p.u. area load), and generation regulation cost (cg in \$/h p.u. area load).

while exports are largely unchanged. We note that at very high FADR levels cost and generation are reduced more significantly while exports are impacted more clearly. This suggests that further study of the system behavior at very high levels of demand response may be desired in the future

5. Discussion

Using the closed-loop system model GK we can compare the proposed control policy's contribution to improving in area control robustness to uncertainty in the availability of fast-acting demand response at the time of a generation contingency. Uncertainty in controllable load can be very large and results from significant diurnal and seasonal variations in the load composition [31]. Fast-acting demand response is typically associated with heating, cooling, and more recently vehicle charging loads because they are flexible in the short term and are usually a significant fraction of the total load at peak times when generation contingencies pose a greater threat to overall system reliability.

5.1. Robustness to FADR Uncertainty

The robustness of the $\mathcal{H}_2$-optimal control policy relative to the conventional ACE control in the presence of highly varying levels of FADR is apparent from Fig. 12. This result is highly significant, particularly when used in the context of FADR to mitigate high penetration of renewables. Increasing renewable resources are associated with declining system inertial response [32] and can lead to more rapid degradation in system stability. As previously discussed, increased FADR can also contribute to deteriorating system stability margins [30]. So while FADR can mitigate renewable intermittency in terms of temporarily relieving thermal generating units from having to quickly ramp, it cannot be concluded that FADR necessarily improves short term system stability without additional measures being applied to the area control policy. The initial results for high-levels of FADR suggest that this is indeed the case and that at the very least the conventional ACE control policy must be reexamined as increasing level of uncontrollable renewable generation are used and FADR is employed to mitigate the impact.

A further consideration is the selection of the FADR design condition. In this study a 5% FADR level was used. The performance of the new control policy using this design condition is quite robust for a wide range of FADR levels. However, it should be recognized that the new control policy is optimal only when the FADR level is close to 5%. At other levels of FADR availability the performance would be suboptimal, although it remains still much better than the conventional ACE control policy, as the cost and energy savings in Table 1 demonstrate. This suggests that careful consideration should be given to the choice of FADR design conditions, especially with respect to (1) the probability distribution of FADR levels over the course of time, (2) the probability of a generation contingency occurring over the course of time, and (3) the relative cost impacts of those contingencies.

It is significant that the new control policy relies only on measurement of import/export power from the control area. For the control policy to be effective, these measurements must be made at very high rate compared to the SCADA measurement rate of 0.25 Hz for ACE. Based on the very fast response rate of the loads, a measurement rate similar to that of phasor measurement units (PMUs) may be necessary for the proposed area control policy. Most PMUs can sample phase angles at 60 Hz, and are capable of point-on-wave measurements in excess of 1000 Hz. However, the control design would have to consider the communications latency from the remote PMUs to the control area's

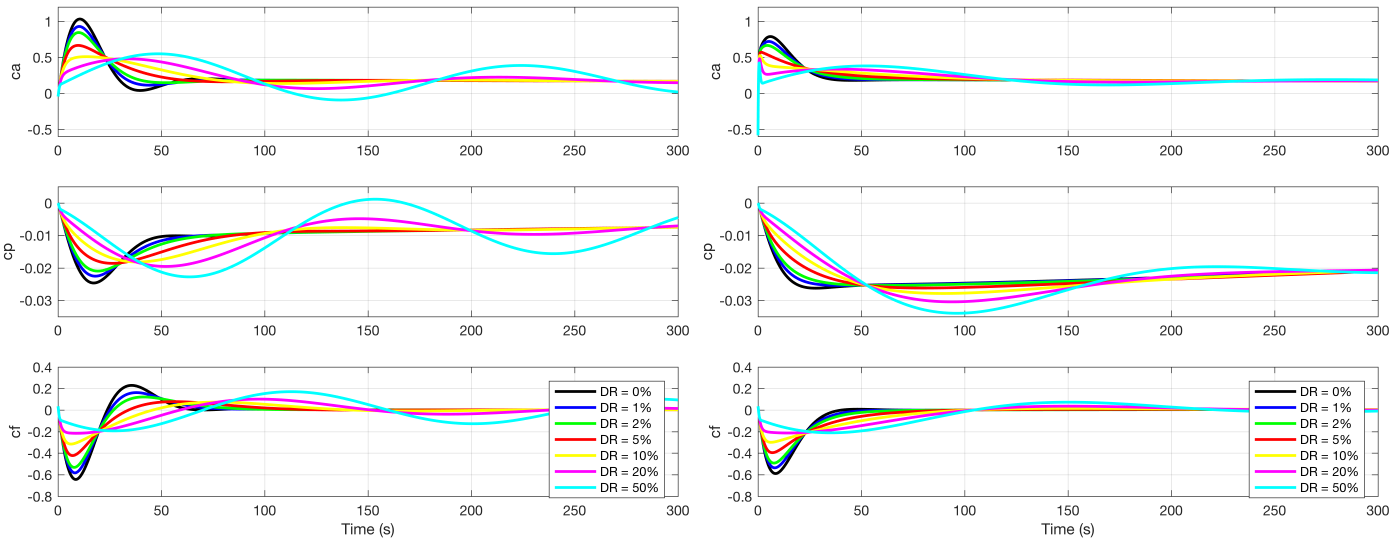

Figure 12: ACE control (left) and $\mathcal{H}_2$-optimal control (right) cost and dispatch for varying demand response levels, where c_a is the total control cost (in \$), c_p is the power control response cost (in \$), and c_f is the frequency control response cost (in \$).

Table 1: Cost, generation, and net export impacts of ACE control versus $\mathcal{H}_2$-optimal control

	Cost			Generation			Exports		
FADR (%)	ACE ($)	$\mathcal{H}_2$ ($)	Saving (%)	ACE (MWh)	$\mathcal{H}_2$ (MWh)	Reduction (%)	ACE (MWh)	$\mathcal{H}_2$ (MWh)	Change (%)
0	13750	13443	2.2	13.75	13.44	2.2	13.75	13.75	0.0
1	13734	13389	2.5	13.73	13.39	2.5	13.75	13.79	-0.3
2	13736	13382	2.6	13.74	13.38	2.6	13.75	13.79	-0.3
5	13754	13427	2.4	13.75	13.43	2.4	13.75	13.77	-0.1
10	13761	13469	2.1	13.76	13.47	2.1	13.75	13.74	0.1
20	13822	13451	2.7	13.82	13.45	2.7	13.76	13.82	-0.4
50	14264	13369	6.3	14.26	13.37	6.3	13.81	14.33	-3.7

data concentrator [33]. PMU technology and availability is evolving rapidly and the deployment of the PMUs under the North America Synchrophasor Initiative (NASPI) has considered the possibility of such a requirement in the design and implementation of the current synchrophasor network [34].

5.2. Future Work

This work has considered only local disturbances, i.e., loss of generation originating within the same generation control area. It will be necessary to consider a wide range of additional disturbances including

1. An internal loss of load (note that this is not equivalent to a negative loss of generation because the responsive resource mix changes),
2. An external loss of generation or load,
3. A loss of a tieline between generation control areas, and
4. Rapid ramp up and down, both internally and externally, due to unexpected changes in renewable resources.

In addition, the new control policy must address the impact of eliminating direct observation of system frequency from the measurement. The role of the secondary generation is to cancel the steady-state frequency deviation and each area's net exports bring back to the scheduled value, either with ACE or $\mathcal{H}_2$-optimal control. A component of the $\mathcal{H}_2$-optimal area generation control minimizes the frequency deviations so it will cope with some, but not necessarily all of the steady-state frequency deviation. It seems unlikely that such a change to the area control policy could go unnoticed, particularly in the event that system inertia and damping change significantly in a short time. Although generation droop remains in effect for all controlled generating units that do not have a master controller, the slow diminution of droop-only units could lead to situations where there is slow or inadequate control of system frequency even though there is very authoritative control of inter-area power exchanges.

This study examined an extreme case in which 75% of the generation was uncontrolled renewable and only 25% of the generation was regulated using the area control policy. For one thing such a great percentage of renewables means

the system does not have enough inertia to deal with both renewable and load uncertainty, so the existing automatic generation control (AGC) system (frequency droop plus ACE) is unable to adequately control the system. Although we used $M = 6$ seconds in this study, it is perhaps still too large. We expect that much lower total system inertias should be considered, perhaps as low as $M = 2$ seconds. With system inertia so low it seems even more likely that control areas will require an augmented or entirely new control policy. With $M = 2$ the advantage of $\mathcal{H}_2$-optimal ACE control may be more evident.

In North America, balancing authorities are scored based on how well they contribute to interconnection frequency regulation needs while tracking their export schedule. The optimal response as presented here does not consider how often "zero-crossings" of nominal frequency occur or how noisy frequency control is. Future studies of optimal-ACE policies considering fast-acting demand response control design will need to also consider the control performance standards CPS-1 and CPS-2.

6. Conclusions

In the paper we have presented a $\mathcal{H}_2$-optimal approach to synthesizing the control policy for control areas in bulk electricity interconnections. The approach is suited to controlling both generation and demand response in areas that have a high penetration of both intermittent renewable resources and fast-acting demand response. The implementation of the $\mathcal{H}_2$-optimal control policy is compatible with, and indeed depends on the transactive control 5-minute dispatch strategy such as were demonstrated on the Olympic Peninsula GridWise and the Northeast Columbus RTPda gridSMART demonstration projects [4].

The transactive $\mathcal{H}_2$-optimal area control policy is shown to be superior to the conventional ACE control policy in that it is (1) significantly more robust to uncertainty in the amount of fast-acting demand response that is available, (2) always less costly and less energy intensive, and (3) minimizes deviation from any surplus maximizing schedule.

Acknowledgments

This work was funded by the Pacific Institute for Climate Solutions (PICS) and by the Laboratory Directed Research and Development program under the Control of Complex Systems Initiative at Pacific Northwest National Laboratory, which is operated for the US Department of Energy by Battelle Memorial Institute under Contract No. DE-AC05-76RL01830. This paper is publication no. 16898 by SLAC National Accelerator Laboratory, which is operated for the US Department of Energy by Stanford University under Contract No. DE-AC02-76SF00515.

Nomenclature

$\Delta_e(t)$	Area net power exports deviation in MW.
$\Delta_f(t)$	System frequency deviation in Hz.
$\hat{f}(s)$	Interconnection frequency response in s-domain.
$\hat{f}(s)$	System frequency in s-domain.
$\hat{g}_d(s)$	Droop-controlled generation response in s-domain.
$\hat{g}_r(s)$	ACE-controlled generation response response in s-domain.
$\hat{l}(s)$	Load response in s-domain.
$\hat{p}(s)$	Interconnection power response in s-domain.
$\hat{s}_s(s)$	Filtered ACE signal in s-domain.
$\kappa_g(kt_d)$	Slope of the generation supply curve at the dispatch point in \$/MW^{2}h.
$\kappa_l(kt_d)$	Slope of the load demand curve at the dispatch point in \$/MW^{2}h.
$\psi(t)$	Regulation energy price in \$/MWh.
$a(t)$	Raw ACE signal in MW.
B	Frequency control bias in MW/Hz.
D	Interconnection damping constant.
$d_p(t)$	Disturbance magnitude in MW.
$e(t)$	Actual net exports from a control area in MW.
e_s	Scheduled net exports from a control area in MW.
$F(s)$	Low-pass ACE control signal filter transfer function.
$f(t)$	System frequency in Hz.
F_d	Fraction of total load that can be responsive to frequency.
F_r	Fraction of generating units that are ACE-controlled.
f_s	Nominal or scheduled system frequency in Hz.
$G_d(s)$	Droop-controlled generation response transfer function.
$G_r(s)$	ACE-controlled generation resource transfer function.
$H(s)$	Interconnection overall transfer function.
K_d	Fraction of total load that is armed by 5-minute dispatch.
K_l	Load control recovery time constant in seconds.
K_p	Load quasi-steady rebound response time constant in seconds
$L(s)$	Load transfer function.
M	Interconnection inertial constant.
R	Droop control constant.
s	Complex frequency variable.
t	Real time variable in seconds.
T_f	ACE control signal filter time constant in seconds.
T_g	Generation resource governor time constant in seconds.
T_l	Load control derivative response gain.
T_{ch}	Generation resource steam chest time constant in seconds.

References

[1] S. Behboodi, D. P. Chassin, C. Crawford, N. Djilali, Renewable resources portfolio optimization in the presence of demand response, Applied Energy 162 (2016) 139–1418.

[2] C. ISO, California iso demand response and energy efficiency roadmap: Maximizing preferred resources (December 2013).

[3] D. J. Hammerstrom et al., Pacific Northwest GridWise Testbed Projects: Part 1. Olympic Peninsula Project, PNNL Report no. 17167, Pacific Northwest National Laboratory, Richland, Washington.

[4] S. E. Widergren, K. Subbarao, J. C. Fuller, D. P. Chassin, A. Somani, M. C. Marinovici, J. L. Hammerstrom, AEP Ohio gridsmart demonstration project real-time pricing demonstration analysis, PNNL Report 23192.

[5] A. K. Bejestani, A. Annaswamy, T. Samad, A hierarchical transactive control architecture for renewables integration in smart grids: Analytical modeling and stability, IEEE Transactions on Smart Grid 5 (4) (2014) 2054–2065.

[6] K. P. Schneider, J. C. Fuller, D. P. Chassin, Analysis of distribution level residential demand response, in: Power Systems Conference and Exposition (PSCE), IEEE, 2011, pp. 1–6.

[7] V. Lakshmanan, M. Marinelli, J. Hu, H. W. Bindner, Provision of secondary frequency control via demand response activation on thermostatically controlled loads: Solutions and experiences from Denmark, Applied Energy 173 (2016) 470 – 480.

[8] J. Zhong, L. He, C. Li, Y. Cao, J. Wang, B. Fang, L. Zeng, G. Xiao, Coordinated control for large-scale EV charging facilities and energy storage devices participating in frequency regulation, Applied Energy 123 (2014) 253 – 262.

[9] S. Falahati, S. A. Taher, M. Shahidehpour, Grid frequency control with electric vehicles by using of an optimized fuzzy controller, Applied Energy 178 (2016) 918 – 928.

[10] F. Teng, Y. Mu, H. Jia, J. Wu, P. Zeng, G. Strbac, Challenges on primary frequency control and potential solution from evs in the future gb electricity system, Applied Energy.

[11] I. Beil, I. Hiskens, S. Backhaus, Frequency regulation from commercial building HVAC demand response, Proceedings of the IEEE 104 (4) (2016) 745–757.

[12] S. Khan, M. Shahzad, U. Habib, W. Gawlik, P. Palensky, Stochastic battery model for aggregation of thermostatically controlled loads, in: IEEE International Conference on Industrial Technology (ICIT), IEEE, 2016, pp. 570–575.

[13] H. Hao, B. M. Sanandaji, K. Poolla, T. L. Vincent, A generalized battery model of a collection of thermostatically controlled loads for providing ancillary service, in: 51st Annual Allerton Conference on Communication, Control, and Computing (Allerton), IEEE, 2013, pp. 551–558.

[14] B. M. Sanandaji, T. L. Vincent, K. Poolla, Ramping rate flexibility of residential HVAC loads, IEEE Transactions on Sustainable Energy 7 (2) (2016) 865–874.

[15] H. Bevrani, H. Bevrani, PID tuning: robust and intelligent multi-objective approaches, INTECH Open Access Publisher, 2011.

[16] F. C. Schweppe, R. D. Tabors, J. L. Kirtley, H. R. Outhred, F. H. Pickel, A. J. Cox, Homeostatic utility control, IEEE Transactions on Power Apparatus and Systems PAS-99 (3) (1980) 1151–1163.

[17] D. J. Hammerstrom et al., Pacific Northwest GridWise Testbed Projects: Part 2. Grid Friendly Appliance Project, PNNL Report no. 17079, Pacific Northwest National Laboratory, Richland, Washington.

[18] D. Jay, K. S. Swarup, Demand response based automatic generation control in smart-grid deregulated market, in: IEEE 6th International Conference on Power Systems (ICPS), 2016, pp. 1–8.

[19] P. Kundur, N. J. Balu, M. G. Lauby, Power system stability and control, Vol. 7, McGraw-hill New York, 1994.

[20] N. R. Subcommittee, Balancing and frequency control, Technical document, North American Electric Reliability Corporation (2011).
URL `http://www.nerc.com/docs/oc/rs/NERC Balancing and Frequency Control 040520111.pdf`

[21] A. Annaswamy, T. Nudell, Transactive control – what's in a name?, IEEE SmartGrid Newsletter (September 2015).

[22] J. Fuller, K. Schneider, D. Chassin, Analysis of residential demand response and double-auction markets, in: IEEE Power and Energy Society General Meeting, IEEE, 2011, pp. 1–7.

[23] D. Chassin, S. Behboodi, C. Crawford, N. Djilali, Agent-based simulation for interconnection-scale renewable integration and demand response studies, Engineering 1 (4) (2015) 422–435.

[24] S. Stoft, Power system economics, Journal of Energy Literature 8 (2002) 94–99.

[25] S. Behboodi, D. Chassin, N. Djilali, C. Crawford, Interconnection-wide hour-ahead scheduling in the presence of intermittent renewables and demand response: a surplus maximizing approach, Applied Energy 189 (1) (2017) 336–351.

[26] A. Kiani, A. Annaswamy, A hierarchical transactive control architecture for renewables integration in smart grids, in: 2012 IEEE 51st Annual Conference on Decision and Control (CDC), 2012, pp. 4985–4990.

[27] K. Subbarao, J. Fuller, K. Kalsi, R. Pratt, S. Widergren, D. Chassin, Transactive control and coordination of distributed assets for ancillary services, Pacific Northwest National Laboratory, 2013.

[28] J. C. Doyle, K. Glover, P. P. Khargonekar, B. A. Francis, State-space solutions to standard h/sub 2/and h/sub infinity/control problems, IEEE Transactions on Automatic control 34 (8) (1989) 831–847.

[29] T. Chen, B. A. Francis, Optimal sampled-data control systems, Springer Science & Business Media, 2012.

[30] S. R. Mattix, M. K. Donnelly, D. J. Trudnowski, J. E. Dagle, Autonomous demand response for frequency regulation on a large-scale model of an interconnected grid, in: IEEE Power and Energy Society General Meeting, 2012, pp. 1–8.

[31] D. Kosterev, A. Meklin, J. Undrill, B. Lesieutre, W. Price, D. P. Chassin, R. Bravo, S. Yang, Load modeling in power system studies: WECC progress update, in: IEEE Power and Energy Society General Meeting-Conversion and Delivery of Electrical Energy in the 21st Century, IEEE, 2008, pp. 1–8.

[32] S. Sharma, S. H. Huang, N. Sarma, System inertial frequency response estimation and impact of renewable resources in ERCOT interconnection, in: IEEE Power and Energy Society General Meeting, 2011, pp. 1–6.

[33] R. Lira, C. Mycock, D. Wilson, H. Kang, PMU performance requirements and validation for closed loop applications, in: 2nd IEEE PES International Conference and Exhibition on Innovative Smart Grid Technologies (ISGT Europe), 2011, pp. 1–7.

[34] P. Kansal, A. Bose, Bandwidth and latency requirements for smart transmission grid applications, IEEE Transactions on Smart Grid 3 (3) (2012) 1344–1352.